Electric Power Systems Research 136 (2016) 370–382

Contents lists available at ScienceDirect

Electric Power Systems Research

journal homepage: www.elsevier.com/locate/epsr

Decentralized voltage control of clustered active distribution network by means of energy storage systems

M. Bahramipanah*, R. Cherkaoui, M. Paolone

École Polytechnique Fédérale de Lausanne, 1015 Lausanne, Switzerland

ARTICLE INFO

Article history:
Received 25 September 2015
Received in revised form 11 January 2016
Accepted 13 March 2016
Available online 4 April 2016

Keywords:
Active distribution networks
Clustering
Decentralized control
Energy storage systems
Multi-agent system
Voltage control

ABSTRACT

The paper presents a network partitioning strategy for the optimal voltage control of Active Distribution Networks (ADNs) actuated by means of a limited number of Distributed Energy Storage Systems (DESSs). The proposed partitioning uses a linear programming approach by means of the known concept of voltage sensitivities. Then, two decentralized optimal control algorithms are proposed relying, respectively, on the Thévenin equivalents and a recursive approach. These algorithms are developed using the Multi-Agent System (MAS) concept. With respect to a centralized control algorithm, the aim of the network clustering is to reduce the number of exchanged messages among the clusters when one of the two proposed decentralized control algorithms is adopted. The effectiveness of the two proposed controls is assessed with respect to the performances of the equivalent centralized control using numerical examples composed by the IEEE 13 and IEEE 123 buses distribution test feeders adapted to include stochastic generation and DESSs.

1. Introduction

As known, the increasing penetration of distributed energy resources in active distribution networks (ADNs) triggers different operation challenges caused by the lack of direct control of stochastic and non-stochastic distributed generation (DG) (e.g., [1,2]). In this respect, one of the main problems associated to the massive connection of DG is represented by the quality-of-service (QoS) of ADNs usually associated to the voltage quality [3]. In this respect, there are different approaches to maintain the ADN QoS such as grid reinforcement and/or control of generation/demand. An alternative solution is represented by the use, and control, of Distributed Energy Storage Systems (DESSs). In this respect, the control of DESSs can be achieved either by centralized or decentralized schemes. Each of them has its own pros and cons. Centralized controls involve the centralization of all the information and consequent decisions in a single point. Thus, there is a consequent computation complexity associated to the central information gathering and processing. Also, the centralized control faces difficulties in some applications when global information is not available [4,5]. Furthermore, in the case of a failure of the central supervisor, the control is lost all over the network. In this respect, the question arises whether centralized controls are still the most appropriate. A possible solution is to move from the centralized operation paradigm to the decentralized one by subdividing the network into quasi-autonomous entities defined as areas, zones or clusters (these terms are used as synonyms in the rest of the paper). To this end, starting from the work presented in [6], this paper first discusses the network clustering and, then, two consequent decentralized control strategies. Both network clustering and decentralized controls make use of a linear programming technique relying on the so-called voltage sensitivity coefficients (e.g., [7–10]).

In this paper, the locations of DESSs are considered to be given and provided by the process described in [11]. Indeed, the cost of using DESSs for controlling ADNs has been already treated by [11] where the Authors have proposed a solution to the problem of DESSs optimal planning accounting for the investment and operation costs of these systems. Thus, the paper assumes to regulate each zone by a controller situated inside each DESS. As a result, it can be considered that the influence of the DGs on the grid is indirectly regulated by the controllers already available into the DESSs. In order to define a decentralized control scheme and to decrease the communication costs and computation burden, two assumptions are made: (i) the operating information within each zone is not shared with the others and (ii) each zone is independently controlled by dedicated single device whose control variables are the active and reactive power set points of a DESS unit. It is assumed that each zone does not contain any directly-controllable generator, or load, except a unique DESS unit.

* Corresponding author. Tel.: +41 21 693 4617; fax: +41 21 693 4662.
E-mail address: Maryam.bahramipanah@epfl.ch (M. Bahramipanah).

http://dx.doi.org/10.1016/j.epsr.2016.03.021
0378-7796/

Nomenclature

DESS^{A_h}	distributed energy storage system located in area A_h
t	index of time
i, j, d	index of node
V_j	voltage of node j
$\mathrm{VSC}_{i\to j}$	voltage sensitivity coefficient of node i on node j
$\mathrm{VIF}_{i\to j}$	voltage influence factor of node i on node j
$\alpha_{i\to j}$	electric resistance line distance between node i and j
$\beta_{i\to j}$	electric reactance line distance between node i and j
IID	independent and identically distributed
DA^{A_h}	DESS agent in area A_h
$\mathrm{CBB}^{Ah,g}$	common boundary bus between area A_h and area A_g
$V_{\mathrm{ref}}^{A_h}$	node voltages reference values
$\overline{V}_{d,t}^{A_h}$	voltage of node d in area A_h at time t
$P_{\mathrm{DESS}}^{A_h}$	active power produced/absorbed by the DESS in area A_h at time t
$Q_{\mathrm{DESS}}^{A_h}$	reactive power produced/absorbed by the DESS in area A_h at time t
$S_{r,\mathrm{DESS}}^{A_h}$	rated power of the converter of DESS^{A_h}
SoC^{A_h}	state-of-charge of DESS in area A_h at time t
$\mathrm{SoC}_{\mathrm{ref}}^{A_h}$	SoC reference value for DESS^{A_h}
$\mathrm{SoC}_{\mathrm{min}}^{A_h}$	minimum SoC for DESS^{A_h}
$\mathrm{SoC}_{\mathrm{max}}^{A_h}$	maximum SoC for DESS^{A_h}
$\overline{V}_{\mathrm{th}}$	Thévenin voltage equivalent
$\overline{Z}_{\mathrm{th}}$	Thévenin impedance equivalent
$\tilde{S}_{\mathrm{CBB}}^{A_h,g}$	equivalent apparent power flowing from area A_h to A_g
N^*	number of the internal buses in A_h including CBBs
$\overline{Y}$	admittance matrix of area A_h
$\overline{V}_s^{A_h}$	voltage of the area A_h virtual slack node
n^{A_h}	Level number of the considered DA^{A_h}
Γ^{A_h}	set of internal states of the area A_h
$S_s^{A_l}$	losses plus supply-demand power mismatches in the considered area A_l
γ^{A_h}	status of DA^{A_h}

The paper is organized as follows: Section 2 summarizes the methods proposed in the literature for the network clustering. Then, the proposed clustering algorithm is presented. Section 3 first presents different control schemes for ADNs and then illustrates two proposed decentralized control algorithms and the associated message exchange processes. Section 4 presents the performance assessment of the decentralized control algorithms making reference to the IEEE 123 node test distribution feeder. The effectiveness of the control algorithms is assessed comparing their performances with those of the equivalent centralized control problem.

2. Network clustering

2.1. Literature review

The partitioning of electrical networks can be approached in several ways. A collection of zones of variable size has been proposed in [12] where supply/demand are kept balanced in order to efficiently control dispatchable DGs. The fluctuations in supply/demand (such as peak/off-peak load variations) change the boundaries of the zones. The drawback of this method is that all the buses need to belong to all possible areas. Further, it requires the direct control of each DG unit. In [13] it has proposed a partitioning algorithm using the so-called community detection theory. It is assumed that the network is initially decomposed in pre-defined areas. Then, the algorithm tries to merge them while the local reactive power balance inside the resulting areas is not fulfilled. In this approach, the voltage is controlled only by adjusting the reactive power neglecting the fact that voltage variations in distribution networks may depend also on active powers as a function of the R/X ratio of lines longitudinal parameters [14].

2.2. Proposed clustering technique

The main hypothesis of the partitioning process and the consequent control algorithms presented in this paper is that DESSs are the only controllable devices in the targeted ADN. In order to decouple the voltage control among a set B ($\dim\{B\} = B$) of DESSs optimally located in a balanced and radial ADN, the proposed partitioning algorithm decomposes the ADN into several quasi-autonomous zones, each one under the control of a single DESS. Therefore, the boundaries of each area are determined with this criterion: each DESS within a zone of unknown extension must have significant influence on the co-zonal controlled variables (in our case the node voltages) in comparison with the nodes outside the zone of interest. In order to achieve such goal, there is the need to quantify the influence of the control variables (i.e., nodal power injection/absorptions of each DESS) on the controlled ones, namely the node voltages. The use of linear programming through voltage sensitivity coefficients (VSC) is used for this purpose (e.g., [7,15]). As known, VSC depends on the topology and the operating state of the grid. In this study, it is relied on the method presented in [7] to compute the VSCs. Given a certain operating state of the network, $\mathrm{VSC}_{i\to j}$ quantifies the change on the voltage at node j for a variation of the injected/absorbed active/reactive powers at node i.

The steps of the proposed heuristic decomposition algorithm are described hereafter.

Step 1. Computation of the VSC matrices: for a given network operating state Γ[1], two sensitivity matrices are computed for both active and reactive powers ($[\mathrm{VSC}^P]_{B\times N}$ and $[\mathrm{VSC}^Q]_{B\times N}$). The relevant elements can be formally defined as in (1) (N is the number of network nodes and B the number of DESS units).

$$\mathrm{VSC}_{i\to j}^{P} = \frac{\partial V_j}{\partial P_i}\Big|\Gamma\ ; \quad \mathrm{VSC}_{i\to j}^{Q} = \frac{\partial V_j}{\partial Q_i}\Big|\Gamma\ ; \quad i \in B; \quad j \in N \tag{1}$$

Step 2. Assessment of the DESSs voltage influence factors (VIF): the VIF of a generic DESS located at node i on node j is defined as the ratio of a given VSC defined by (1) and the scalar sum of all VSCs. As a result, two influence matrices ($[\mathrm{VIF}^P]_{B\times N}$ and $[\mathrm{VIF}^Q]_{B\times N}$) are derived by using the following equation:

$$\mathrm{VIF}_{i\to j}^{P} = \frac{\partial V_j/\partial P_i}{\sum_{n=1}^{N}\partial V_n/\partial P_i}\Big|\Gamma\ , \quad \mathrm{VIF}_{i\to j}^{Q} = \frac{\partial V_j/\partial Q_i}{\sum_{n=1}^{N}\partial V_n/\partial Q_i}\Big|\Gamma \tag{2}$$

Step 3. Merge matrices $[\mathrm{VIF}^P]_{B\times N}$ and $[\mathrm{VIF}^Q]_{B\times N}$: the use of (2) allows to infer two matrices $[\mathrm{VIF}^P]_{B\times N}$ and $[\mathrm{VIF}^Q]_{B\times N}$. In order to have a more compact indicator considering both effects of active and reactive powers of DESS simultaneously, it is proposed to merge these two matrices in a single one $[\mathrm{VIF}]_{B\times N}$. For this purpose, a linear relationship is built based on the concept of the electric distances using (3).

[1] Γ represents the set of the phasors of the ADN phase-to-ground nodal voltages at a given time [31]

$[\mathrm{VIF}^P]_{B\times N}$ and $[\mathrm{VIF}^Q]_{B\times N}$ are weighted by the corresponding resistance and reactance electric distance between the nodes, respectively. This can be easily proven numerically as shown in the appendix.

$$[\mathrm{VIF}]_{B\times N} = [\alpha]_{B\times N} \times \left[\mathrm{VIF}^P\right]_{B\times N} + [\beta]_{B\times N} \times \left[\mathrm{VIF}^Q\right]_{B\times N} \quad (3)$$

Each element of $[\alpha]_{B\times N}$ and $[\beta]_{B\times N}$ are defined as in the following equation:

$$\alpha_{i\to j} = \frac{\left(\sum R_{ij}\right)^2}{\left(\left|\sum \bar{Z}_{ij}\right|\right)^2}; \quad \beta_{i\to j} = \frac{\left(\sum X_{ij}\right)^2}{\left(\left|\sum \bar{Z}_{ij}\right|\right)^2}; \quad \alpha+\beta=1 \quad (4)$$

where $\sum R_{ij}$, $\sum X_{ij}$ and $\sum Z_{ij}$ are respectively the sum of the line resistances/reactances/impedance of the lines between node i and node j. As a result, a single matrix $[\mathrm{VIF}]_{B\times N}$ is obtained.

Network node clustering with respect to the DESS units: as anticipated, only one DESS per area is considered. For each node, the DESS that has the most impact is determined by finding the maximum component value of each column of the matrix $[\mathrm{VIF}]_{B\times N}$. More precisely, each node is assigned to the area associated to the DESS with the highest VIF on that node. In this way, it is guaranteed that each node belongs to one and only one area.

It should be noted that the VSCs computation at each time step requires solving a central load flow problem. Deterministic load flow ignores uncertainties in power systems nodal power fluctuations (i.e., those of DG and loads). Whereas it is expected that such uncertainties would change the frontiers of the zones. Actually, changing the borders accordingly (dynamic partitioning) contradicts the assumption that each zone should independently control its area without sharing any information with the neighbors. In order to take into account this aspect, different mathematical approaches can be used, such as the probabilistic approach, fuzzy sets and interval analysis. Probabilistic Load Flow (PLF) (e.g., [16]) has been applied instead of a classical deterministic load flow in order to consider the possible combinations of loads/generations. The PLF requires a priori knowledge of the probability distribution functions (PDF) of the nodal powers injections/absorptions together with their time covariance. In order to infer this statistical information, a set of experimental data (available for a time period of one year) obtained from a real ADN located in the south-east region of Switzerland is used. For each time period t^* (in our case t^* corresponds to a slot of 15 min) of a given day d, the empirical Cumulative Distribution Function (CDF_{d,t^*}) of nodal powers is built using all the measurements collected at t^* in correspondence of $d-15$ and $d+15$. 96 CDFs of active/reactive powers per day per node are obtained. From the knowledge of the nodal CDFs, the PLF is solved numerically using a Monte Carlo simulation (MCS) (e.g., [17]). For this purpose, the nodal powers are assumed as IID variables. It is worth noting that since the electric distances between the system nodes are considered in the proposed clustering method using (3), the nodes always tend to be remain in the area corresponding to the closest DESS. In addition, a PLF have been performed for an entire year to infer the VIF of DESS powers on the grid nodal voltages. Thus, all the possible combinations of loads/generations as well as the uncertainties of the stochastic resources are considered.

2.3. Illustrative example

In order to illustrate the partitioning algorithm, an example is presented in this part referring to the IEEE 13 nodes distribution test feeder. It is supposed to have non-dispatchable DG units composed

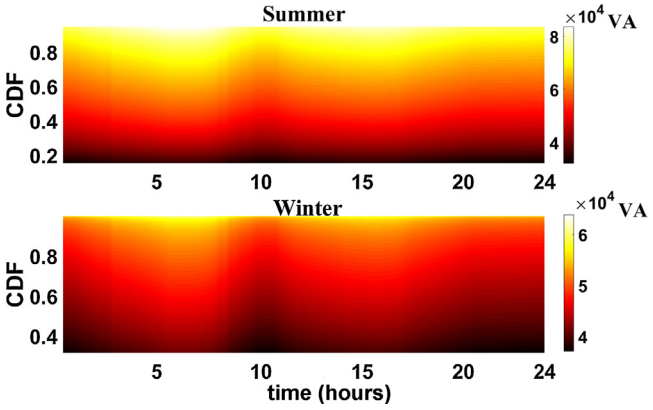

Fig. 1. CDFs of load apparent power during summer and winter for node 9 of the network shown in Fig. 4.

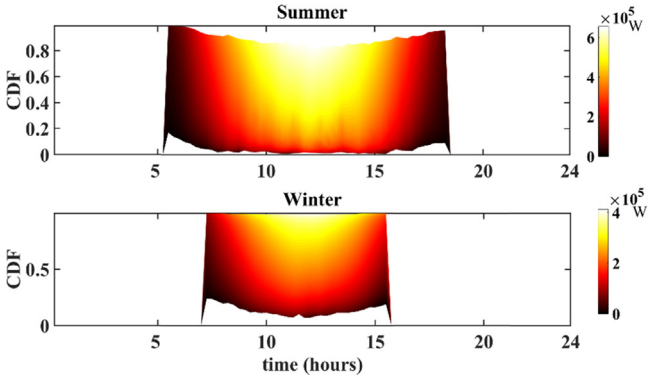

Fig. 2. CDFs of PV power generation during summer and winter for node 9 of the network shown in Fig. 4.

of photovoltaic panels (PVs) (on nodes 4, 8 and 10). The power injections of PVs are represented by voltage-independent active power injections with the null reactive component. Concerning the representation of the network loads, they are considered as voltage independent PQ absorption. Three DESSs (on nodes 6, 4 and 12) are optimally placed located.

Figs. 1 and 2 show, respectively the CDFs of the load apparent power absorptions and PV active power injections for a summer and a winter day for the node 9 of the benchmark grid of Fig. 4. The PLF is performed along 1 year by generating 10,000 runs per 15 min. The obtained minimum/maximum variations of the VIF for the three DESS are plotted in Fig. 3. As it is seen, the nodes with the highest VIF belongs to the corresponding area where the associated

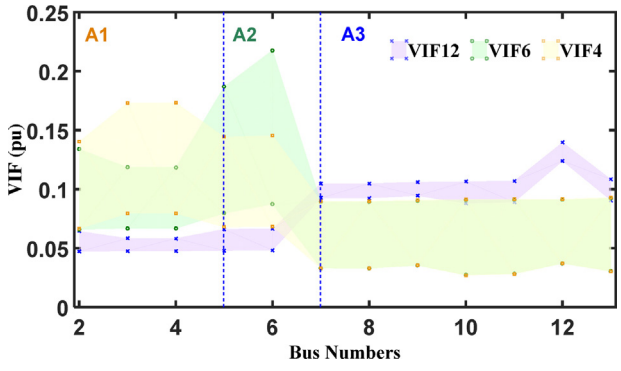

Fig. 3. Annual range of VIF of DESSs on all nodes of 13 bus system.

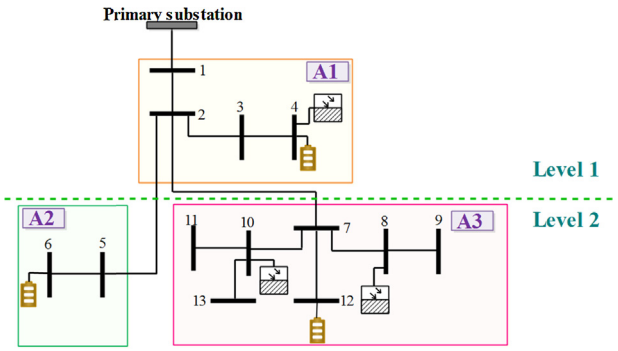

Fig. 4. Clustered IEEE 13 nodes test system.

DESS is located. The network schematic and the obtained zones decomposition are shown in Fig. 4.

3. Proposed voltage control method

Due to the increasing penetration of DGs, the issue of voltage regulation of ADNs becomes more significant. Several methods have been proposed in the literature to overcome this issue including centralized and decentralized schemes [5–18].

In the centralized control framework, all the information and consequent decisions are accumulated in a single point. Although the centralized control strategy is the most straightforward way to achieve the management of the network, it has several drawbacks: (1) there is a consequent computation complexity associated to the central information gathering/processing. (2) It faces difficulties in some applications when global information is not available [19]. (3) In the case of a failure of the central supervisor, the control is lost all over the network. (4) It needs high investment in communication and data processing. Due to the above-mentioned downsides, decentralized control schemes have been proposed. In these approaches, the controllable devices are autonomous, and the control decisions could be made according to the local information only [20]. Decentralized voltage control using the DGs' inverters has been proposed, for instance, in [20,21]. However, the optimal coordination of hundreds of inverters might require a complex telecommunication infrastructure leading to high investment costs. In addition, the active power control by DGs might be not permitted due to the existing grid code for prosumers. Thus, in the network characterized by high ratios' R/X of longitudinal line impedances, the reactive power compensation relying on those DGs' inverters could not be sufficient to achieve satisfying voltage control. OLTC is used in [22] in order to control the grid voltages in a distributed manner. However, the structure of the feeders affects the effectiveness of this method significantly. [23] proposed a decentralized control method based on consensus protocol. In this approach, the distribution system operator should install extra controllers/agents in some specific buses which impose extra costs. [20–24] used network equivalents to achieve decentralized control. The decentralized scheme can be modeled using recursive procedures taking advantage of the hierarchical structure of the grid [24,25]. Using the clustering technique presented in Section 2, in this paper, the regulation of zonal node voltages is done by the controllers situated inside each DESSs. Thus, unlike the consensus methods, no extra controller is needed to be installed. Moreover, with this assumption, the influence of the DGs on the grid is indirectly regulated by the controllers already available in the DESSs. Thus, the peculiarity of distributed control in multi-area systems is that the internal state of each area is not shared with the others. In what follows the architecture and the formulation of two decentralized control methods based on network equivalent models and the recursive approaches are illustrated.

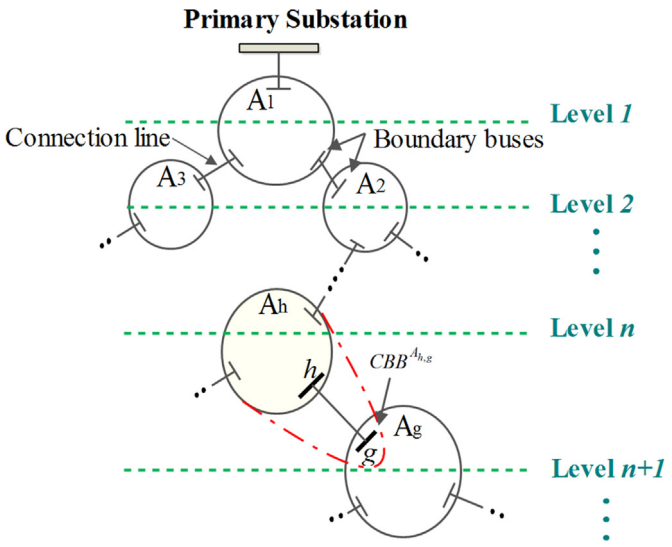

Fig. 5. Representation of CBBs in the clustered network with the area level numbers allocation.

3.1. Multi agent system structure

According to the clustering method presented in Section 2, the whole distribution network is divided into K areas; each one including only one DESS. This consideration introduces the idea that the voltage control problem might be solved in a distributed manner. Therefore, each area should have zonal control capability. For this purpose, an agent is assigned to each area which is called "area agent". The zonal control is implemented using multi-agent system (MAS) concept. MAS is one of the most convenient approaches distributing the control in a large-scale system. MAS is composed by multiple intelligent agents that are able to process the data and make the decision in a distributed manner [23–26]. All the interactions between agents take place via a form of message passing. The Foundation for Intelligent Physical Agents (FIPA) defines agent's communication in terms of a function, or action called Communicative Act. There are several type of exchanged messages. Some of them are used in this paper:

INFORM: the sender informs the receivers that some actions are performed. It also sends its new updates.

REQUEST: the sender requests the receivers to perform some actions.

CONFIRM: the sender informs the receivers that a given proposition is true, where the receiver is known to be uncertain about the proposition.

3.2. Proposed decentralized control methods

In this study, the proposed zonal control capability is based only on voltage control since the frequency is dictated by the upper transmission network. Due to the hypothesis of the radial structure of the considered ADN and the partitioning features, there is only one connection line between any two adjacent areas. An abstract representation of a clustered network is shown in Fig. 5. Since there is only one controllable DESS in an area, the area agent is dedicated to the related DESS which is called "DESS Agent" (DA). DAs have a full vision on their own areas with reference to the state of their related DESS unit, and area loads/generations. In fact, the recent literature has discussed the possibility to use dedicated

metering infrastructures for ADNs monitoring and control functionalities (e.g., [27]). In this respect, the use of smart meters in distribution networks allows each DA to have access to the aggregated nodal power consumption data. Therefore, we assume that DAs have the information to carry out a local load flow (or a state estimation) in order to compute the nodal voltages. However, each DA is supposed to share no information about its area with the other DAs except the information at the boundary buses. In this respect, for a given pair of adjacent areas, one of them is extended to include the boundary node of the other (in Fig. 5, area A_h is extended to include bus g of area A_g, which is one of its neighbors). Node g is defined as the common boundary bus ($CBB^{A_{h,g}}$) of both areas A_h and A_g. As a result, between any two adjacent areas one node is selected as CBB. It should be noticed that the CBB is registered within both relevant DAs.

It should be noted that in case of any changes in the topology of the network, the clustering method should be re-performed and each node can be reassigned to a new associated area. In this respect, it is worth observing that ADNs are characterized by the presence of a limited number of breakers resulting into a finite number of different topologies. The distribution system operator might run the proposed clustering algorithm offline for each of them in order to find the extension of each zone for each topology.

3.2.1. General principles

In this paper, two different decentralized control methods for multi-area ADN are proposed corresponding to each solution techniques groups mentioned earlier. They are called: "Thévenin-based" and "Top-down sweep" control methods respectively. In both of them, DAs try to keep the area nodes voltages close to the desired values by carrying out the voltage control locally. The agent DA in each area determines the DESS operating point (i.e., its active, reactive power set-points) without the explicit knowledge of the data of adjacent areas, being only necessary to exchange the CBBs information. A major difference between them is related to the interactions among DAs with respect to the messages exchanged.

In the "Thévenin-based control method", DAs interact each other indirectly through a Coordination Agent (CA). In this respect, each DA provides to the CA a Thévenin equivalent model seen from each of its CBBs as well as the voltage value of each CBB. Based on these inputs, the CA takes care about the coordination between all the DAs tasks.

It is important to notice that CA is not a central controller. It does not have full vision of the entire state of the network, but it has the knowledge of all the CBBs IDs and their respective state variables (voltages).

The "Top-down sweep control method" is based on a recursive approach. The architectural model of the message exchange of this second approach is peer to peer (p2p) as any agent is able to initiate communication with its adjacent one or to be the subject of an incoming communication at any time from those adjacent agents. Therefore, unlike the previous method, DAs interact directly without the need for any CA. In this approach, a level number is assigned to each area in such a way that the area including the main slack bus of the system (primary substation) receives the level number equal to 1. All other areas are leveled from top to down successively due to the radial structure of the distribution network. Once an area gets a level number ($n+1$), the adjacent downstream areas are the next ones that are given the level numbers (n). In Fig. 5, the allocation of the level number to each area is shown as an example. Thus, A_1 has the level number equal to 1. After that, A_2 and A_3 have the next level numbers that is 2. It is worth noting that this process relies uniquely on the radially of the system topology. Therefore, if this condition holds, it can be extended to any distribution networks including also different voltage levels (e.g., medium and low voltage grids).

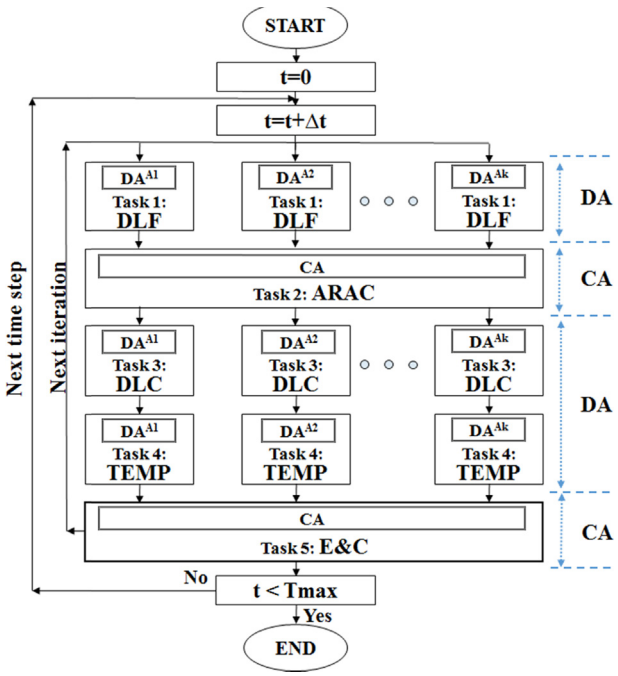

Fig. 6. The general framework of the proposed Thévenin-based distributed control method.

In what follows, both proposed control methods are explained in details.

It should be noted that running PLF for partitioning the grid inherently accounts for the uncertainties of the stochastic resources connected to the system (i.e., loads and stochastic generation). Therefore, the associated computation of VSC accounts for these uncertainties. Alternative ways to treat this problem are illustrated in [28].

3.2.2. Thévenin-based decentralized control method

The general framework of this control method is shown in Fig. 6. The algorithm is performed at each time step by all DAs and CA (being Δt the time step between two subsequent control actions). The proposed control method relies on 5 tasks carried out in sequence. These tasks are described as follows considering a given area A_h.

Task 1. Distributed load flow (DLF) computation by DAs: In order to perform the local load flow in each area, individual slack nodes are randomly selected by the DA^{A_h}. Thus, the load flow can be performed locally. Also, the equivalent complex power at CBBs must be known. Since this power is a priori unknown, it is computed iteratively using the process described below. At each time step, in the first iteration, an initial value is selected for each CBB of an area (i.e., the initial value of the load/generation at this node before the control action). In the subsequent iterations, this complex power is updated thanks to the voltage values resulting from task 3 and the CBBs voltages update provided by task 5.

Task 2. Area Reference Angle Corrections (ARAC) by the CA: In order to comply with the results derived from a centralized control, the CA need to align the voltage angles that each DA has obtained using own slack buses with respect to the main slack node of the system (i.e., the primary substation). The process starts from the top area located at level 1 (since it includes the main reference node) moving towards the bottom areas in the next levels sequentially. At the initialization of this task, the top area is defined as a "principal area" and its direct neighbors as "dependent areas". Then, the

difference of the voltage angles seen from the principal area and the dependent areas are computed by using the following equation:

$$\Delta\delta = \delta_{\text{CBB}}^{\text{dependent}} - \delta_{\text{CBB}}^{\text{principal}} \tag{5}$$

Then, the voltage angle at every node in the "dependent areas" are shifted with the above-mentioned angle difference $\Delta\delta$.

$$\delta_i = \delta_i - \Delta\delta \quad i \in \text{dependent area nodes} \tag{6}$$

In the next steps, every previous "dependent area" becomes, in turn, a "principal area" and its direct neighbors as new "dependent areas". The procedure of angle adjustment in the "dependent areas" propagates downwards until reaching the bottommost area. It is straightforward to conclude that this process works only if the network has a radial topology.

Task 3. Decentralized Local Control (DLC) by DAs: Each DA^{A_h} has now the knowledge of its internal state inferred through the solution of the distributed load flow. Therefore, the VSCs can be computed for both active/reactive powers of DESS located in A_h. It is now possible to formulate a linear-programming optimal control problem (based on the knowledge of VSCs) in order to keep the voltage close to the desired value at each node belonging to A_h. The control variables of the optimization problems are the injected/absorbed active/reactive power of the DESS on the AC-side of their power converters (i.e., $P_{\text{DESS}}^{A_h}$ and $Q_{\text{DESS}}^{A_h}$). The DESS State-of-Charge, SoC^{A_h}, is defined as the remaining energy inside the device assuming, as a first approximation, a unity energy efficiency of the device. In general, SoC is used for electrochemical storage system to indicate the available amount of charge that can be extracted from the system at a given discharge rate. Therefore, this quantity does not explicitly quantify the energy reservoir level of the storage system. In this respect, in this paper the SoC is intended as an indicator of the energy that can be extracted from a generic storage system at any discharge rate. The energy flow is assumed to be positive during the discharge and negative during its charge.

$$\text{SoC}^{A_h}(t) = \text{SoC}^{A_h}(t - \Delta t) + P_{\text{DESS}}^{A_h}(t) \times \Delta t \tag{7}$$

where $\text{SoC}^{A_h}(t-\Delta t)$ is the SoC in the previous time step, Δt is the control time interval and $P_{\text{DESS}}^{A_h}(t)$ the output of the optimal control problem. The objective function and the constraints of the optimal control problem are formulated for each area as (8). In order to get a solution in any case, the inequality constraints associated to the lines ampacities and voltage limits at the nodes are disregarded.

$$\begin{aligned} &\min_{P_{\text{DESS}}^{A_h}, Q_{\text{DESS}}^{A_h}} \sum_{d,t} \left\| \left|\overline{V}_{A_h}^{d,t}\right| - V_{A_h}^{\text{ref}} \right\|^2 + \left(\text{SoC}^{A_h} - \text{SoC}_{A_h}^{\text{ref}}\right)^2 \\ &s.t \quad \text{SoC}_{\min}^{A_h} \le \text{SoC}^{A_h} \le \text{SoC}_{\max}^{A_h} \\ &\qquad {P_{\text{DESS}}^{A_h}}^2 + {Q_{\text{DESS}}^{A_h}}^2 \le {S_{r,\text{DESS}}^{A_h}}^2 \end{aligned} \tag{8}$$

where $\left|\bar{V}_{d,t}^{A_h}\right|$ is the voltage magnitude of node d in A_h at time t ($d = 1,2,\ldots,N^*$). N^* is the number of the internal buses in A_h including the CBBs, $V_{\text{ref}}^{A_h}$ and $\text{SoC}_{\text{ref}}^{A_h}$ are the voltage and SoC reference values, respectively. The constraints for the optimization problem are related to the SoC^{A_h} as well as the capability curves of the power converters assumed to interface the DESS^{A_h} with the grid. In this respect, the $S_{r,\text{DESS}}^{A_h}$ is the rated power of the converter of DESS^{A_h}. The storage devices are not allowed to be charged or discharged completely. The associated limits ($\text{SoC}_{\min}^{A_h}$ and $\text{SoC}_{\max}^{A_h}$) are, in general, defined in order to prevent any damage to the storage system and/or reducing its lifetime.

The voltage at internal bus d could be expressed as its initial value plus a variation provided by the DESS^{A_h}

$$\left|\overline{V}_{d,t}^{A_h}\right| = \left|\overline{V}_{d,t}^{\text{init},A_h}\right| + \Delta\left|\overline{V}_{d,t}^{A_h}\right| \tag{9}$$

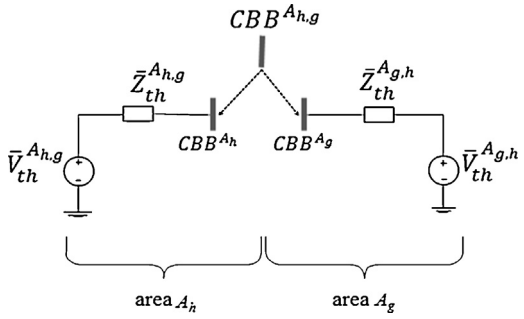

Fig. 7. Thévenin equivalent circuit models seen from $\text{CBB}^{A_{h,g}}$.

where $\overline{V}_{d,t}^{\text{init},A_h}$ comes from the results of DLF task. $\Delta\left|\bar{V}_{d,t}^{A_h}\right|$ is computed by the following (approximated) linear equation:

$$\Delta\left|\overline{V}_{d,t}^{A_h}\right| = \text{VSC}_{b\to d}^{P} \times P_{\text{DESS}}^{A_h} + \text{VSC}_{b\to d}^{Q} \times Q_{\text{DESS}}^{A_h} \tag{10}$$

where b is the node where DESS^{A_h} is located. So, the new voltage values for the internal buses and CBBs are provided by DAs to CA.

Task 4. Computation of Area Thévenin Equivalent Model Parameters (TEMP) by DAs: As mentioned earlier, DAs provide Thévenin equivalent models to the CA. For a given pair of adjacent areas A_h and A_g, the corresponding $\text{CBB}^{A_{h,g}}$ divides the whole network in two distinct sub-grids containing A_h and A_g. It is considered that the $\text{CBB}^{A_{h,g}}$ is split into two virtual buses CBB^{A_h} and CBB^{A_g} associated to A_h and A_g, respectively. It is assumed that each sub-grid is represented by its Thévenin equivalent model seen from the $\text{CBB}^{A_{h,g}}$ (see Fig. 7). The voltage of the $\text{CBB}^{A_{h,g}}$ calculated for A_h is $\overline{V}_{\text{th}}^{A_{h,g}}$; while this voltage calculated for A_g is $\overline{V}_{\text{th}}^{A_{g,h}}$. From the circuit of Fig. 7 the uniqueness of the voltage at the shared CBB can be enforced. If the calculated voltages at $\text{CBB}^{A_{h,g}}$ are different, the algorithm makes the voltage to be unique at this node using the procedure described in Task 5. The Thévenin impedance seen from $\text{CBB}^{A_{h,g}}$ regarding A_h is calculated by using the following equation:

$$\overline{Z}_{\text{th}}^{A_{h,g}} = \frac{\left|\overline{V}_{\text{th}}^{A_{h,g}}\right|^2}{\overline{S}_{\text{CBB}}^{*A_{h,g}}} \tag{11}$$

This equation can be also written for A_g inverting the indices h and g. $\bar{S}_{\text{CBB}}^{A_{h,g}}$ is the equivalent apparent power flowing from A_h to A_g through $\text{CBB}^{A_{h,g}}$ which is calculated using active and reactive injection power equations as follows:

$$P_{\text{CBB}}^{A_{h,g}} = \sum_{d=1}^{N^*} \left|V_{\text{th}}^{A_{h,g}}\right| \left|V_d\right| \left|Y_{\text{CBB}^{A_h},d}\right| \cos\left(\theta_{\text{CBB}^{A_h},d} - \delta_{\text{CBB}^{A_h}} + \delta_d\right) \tag{12}$$

$$Q_{\text{CBB}}^{A_{h,g}} = -\sum_{d=1}^{N^*} \left|V_{\text{th}}^{A_{h,g}}\right| \left|V_d\right| \left|Y_{\text{CBB}^{A_h},d}\right| \sin\left(\theta_{\text{CBB}^{A_h},d} - \delta_{\text{CBB}^{A_h}} + \delta_d\right) \tag{13}$$

$$\overline{S_{\text{CBB}}^{A_{h,g}}} = P_{\text{CBB}}^{A_{h,g}} + j \times Q_{\text{CBB}}^{A_{h,g}} \tag{14}$$

where N^* is the number of the internal buses in area A_h including CBBs; $\overline{Y}$ is the admittance matrix of area A_h. $\left|Y_{\text{CBB}^{A_h},d}\right|$ and $\theta_{\text{CBB}^{A_h},d}$ are the magnitude and phase of the element of the admittance matrix corresponding to row $\text{CBB}^{A_{h,g}}$ and column d. $\delta_{\text{CBB}^{A_h}}$ and δ_d are the voltage phases of $\text{CBB}^{A_{h,g}}$ and bus d, respectively. For a given area the Thévenin impedance and voltage should be computed for each of its related CBBs.

Task 5. Exchange and update of CBBs information and Convergence condition check (E&C) by CA: As mentioned earlier, for each

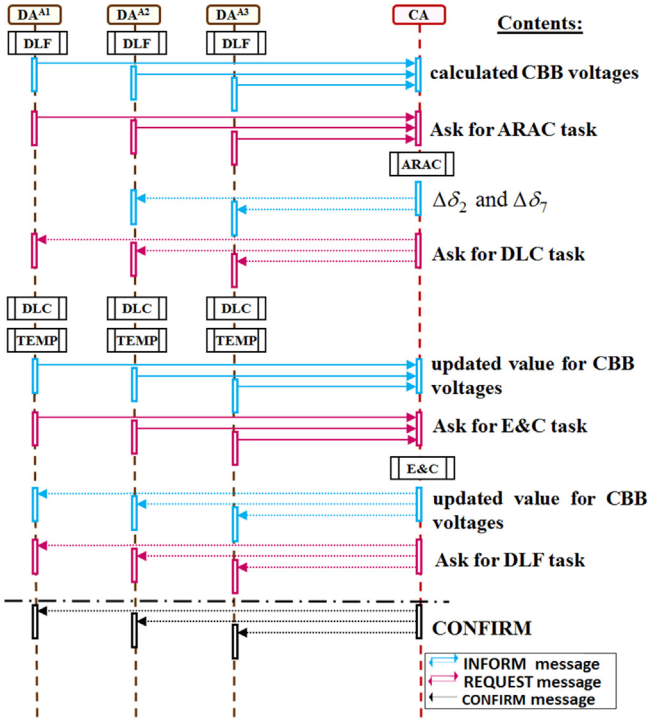

Fig. 8. The sequence diagram for communication procedure for Thévenin-based control method.

pair of adjacent areas the voltage at the shared CBB must be unique. In other words, for a given CBB$^{A_{h,g}}$ linking A_h and A_g, the equality constraint (15) must be respected; where the voltages $\overline{V}_{\text{th}}^{A_{h,g}}$ and $\overline{V}_{\text{th}}^{A_{g,h}}$ are computed separately for A_h and A_g respectively by their related DAs.

$$\overline{V}_{\text{th}}^{A_{h,g}} = \overline{V}_{\text{th}}^{A_{g,h}} \tag{15}$$

The CA first checks for all CBBs whether (15) is simultaneously satisfied. If this is the case, then the distributed control at the current time t converged and the active/reactive DESSs power set points are updated. If it is not the case, the CA forces the voltage at each CBB to be unique using (16). In the proposed control method, the overall optimum solution is achieved iteratively.

$$\overline{V}_{\text{th,new}}^{A_{h,g}} = \overline{V}_{\text{th,new}}^{A_{g,h}} = \frac{\left(\overline{V}_{\text{th}}^{A_{h,g}}/\overline{Z}_{\text{th}}^{A_{h,g}}\right) + \left(\overline{V}_{\text{th}}^{A_{g,h}}/\overline{Z}_{\text{th}}^{A_{g,h}}\right)}{\left(1/\overline{Z}_{\text{th}}^{A_{h,g}}\right) + \left(1/\overline{Z}_{\text{th}}^{A_{g,h}}\right)} \tag{16}$$

3.2.2.1. Illustrative example of DAs and CA message exchange. In order to illustrate the message exchange process between DAs and CA, an example is presented with respect to the IEEE 13 nodes distribution test feeder shown in Fig. 4. Bus 2 and 7 are selected as CBBs between areas A_1 and A_2 as well as areas A_1 and A_3, respectively. The Sequence diagram for communication process among CA and DAs is shown in Fig. 8. The message exchange follows the following sequence.

Sequence 1: DAs perform DLF task.

Sequence 2: DAs send the "INFORM" message to CA accompanying with the calculated values for CBB voltages.

Sequence 3: DAs send the "REQUEST" message to CA asking for ARAC task.

Sequence 4: ARAC task is done by CA when the "REQUEST" message is received from all DAs. The difference of the CBBs voltage angles seen, respectively from each of the areas are computed as the following equation:

$$\Delta\delta_2 = \delta_2^{A_2} - \delta_2^{A_1}; \quad \Delta\delta_7 = \delta_7^{A_3} - \delta_7^{A_1} \tag{17}$$

Sequence 5: CA sends "INFORM" message with the content of the value of the calculated $\Delta\delta_2$ and $\Delta\delta_7$ to DA^{A_2} and DA^{A_3}, respectively.

Sequence 6: CA sends "REQUEST" messages to all DAs asking for DLC and TEMP tasks.

Sequence 7–8: DAs perform DLC and TEMP tasks.

Sequence 9: DAs send "INFORM" messages to CA with the content of the updated values of CBBs voltages.

Sequence 10: DAs ask for E&C check task by sending the "REQUEST" message to CA.

Sequence 11: CA performs E&C task. If the differences of the CBBs voltages calculated by adjacent areas are equal to zero, the procedure goes to the next time step at sequence 14. If this is not the case it goes to sequence 12.

Sequence 12: CA sends "INFORM" message to DAs allowing them to know the updated value of CBB voltages.

Sequence 13: CA asks the DAs for the DLF task by sending the REQUEST message and the procedure goes to sequence 1.

Sequence 14: CA sends CONFIRM message to DAs to let them know about the convergence of the current time step.

The main feature of the proposed method is the independence of the voltage control for each area and the possibility for any area to join into or move back from the control scheme. However, the main drawback is that the process requires the presence of the CA.

3.2.3. Top-down sweep control method

The second proposed control algorithm is a recursive one. In this approach, CBBs are considered as the area slack nodes except the area including the physical slack bus of the system (i.e., the primary substation). For the area with more than one neighbor, the CBB between the area and the adjacent neighbor located at the lower level is selected as the slack bus. First, the approach propagates the Area Local voltage Control (ALC) from the area located at level 1 towards the peripheral ones. In this propagation, the slack node voltage of a given area at the generic level n is imposed by the unique adjacent area at level $n-1$. Then, the algorithm moves from the bottommost areas to the level 1. In this backward motion, the supply-demand power mismatches of a given area (including also the internal area power losses) are transferred sequentially to the main slack node connected to the physical slack.

This process is repeated until the calculated injected power at the main slack node of the system converges to a fixed value. The ALC relies on four tasks. For a given area A_h:

Task 1: Perform distributed load flow. The DAs perform a distributed load flow considering the slack node voltage as indicated earlier as well as the transferred powers calculated from the adjacent areas located at the higher level (see Task 4).

Task 2: VSCs computation. VSCs are computed for both active/reactive powers of DESS^{A_h}.

Task 3: Control of area node voltages. The local voltage control method is the same used in Thévenin-based decentralized control method [i.e., obtained using (8)–(10)].

Task 4: Computation of the area internal power mismatches. As known, the slack node is responsible for providing the power to compensate the losses and the supply-demand mismatches of the system. Since several slack nodes are considered, sharing these mismatches should be avoided by all the area slack nodes. In fact, the area slack nodes are virtual ones that enable DAs to perform the local distributed load flow. Therefore, the area losses, as well as the area supply-demand power mismatches, must be transferred to the real slack node of the system (in general the primary substation). In this respect, each area computes these powers in

correspondence of the virtual slack node. So for area A_h, the slack node powers are computed by using the following equation:

$$P_s^{A_h} - jQ_s^{A_h} = \overline{V}_s^{*A_h} \times \left(\overline{V}_s^{A_h} \sum_{\substack{j=1 \\ j \neq s}}^{N^*} \overline{Y}_{sj}^{A_h} - \sum_{\substack{j=1 \\ j \neq s}}^{N^*} \overline{V}_j^{A_h} \times \overline{Y}_{sj}^{A_h} \right) \quad (18)$$

where $\overline{V}_s^{A_h}$ is the voltage of the A_h virtual slack node and N^* is the number of internal nodes in A_h including CBBs. $\overline{Y}_{sj}^{A_h}$ is the element of the admittance matrix of A_h corresponding to row s (slack) and column j. This calculated power is added to the CBB of the adjacent area located at the lower level as a load.

3.2.3.1. Illustrative example on message exchange. In this control method, the architectural model of the MAS is p2p. The DAs decisions are based on local information as well as those provided by neighbor DAs. In particular, a specific agent, say DA^{A_h}, has access to the following set of information:

$$DI^{A_h} = [n^{A_h}, \gamma^{A_h}, \Gamma^{A_h}] \quad (19)$$

$$N^{A_h} : \left\{ \vartheta^{A_h,l} \right\}; \quad \vartheta^{A_h,l} = \left[n^{A_l}, V_{CBB}^{A_l}, S_s^{A_l} \right] \quad (20)$$

where n^{A_h} is Level number of the considered DA^{A_h}; Γ^{A_h} is set of internal states of the area A_h (in particular, nodes voltages, losses, etc.); $S_s^{A_l}$ is losses plus supply-demand power mismatches in the considered area A_l; $V_{CBB}^{A_l}$ is the voltage of the CBB node between area A_h and A_l and γ^{A_h} is DA^{A_h} status which has two modes; named SL and LS whose meaning is given by the proposition here below. Based on the level number and the area current status, a given DA defines which adjacent DAs to communicate with and which information should be exchanged, using the following proposition.

Proposition #1—A given area with the current status of SL at level χ can communicate only with the adjacent areas with the level number $\chi + 1$ and the exchanged information between them is the voltages of the related CBBs. The area with the current status of LS at level χ can just communicate with the only adjacent one with the level number $\chi - 1$; and the exchanged information between them are the area losses and the area power mismatches.

Each area changes its status considering the received information from the adjacent ones. Receiving updated values for slack node voltage results in SL mode; while receiving updated values for S_s computed by (18), results in LS mode. It should be noted that the DAs located at the lowest and highest levels in the system do not change their statuses since they are always with SL and LS statuses respectively. In addition, the updated S_s values should be received from all adjacent DAs with LS status in order to let the specific DA fulfills its tasks.

At the current time t, the Top-down sweep control method starts the control process from the area with the level equal to 1. Then, the algorithm pursues the following general procedure for a given area A_h at level n.

Step 1: the local voltage control (ALC) is performed by DA^{A_h}. The set DI defined by (19) is updated.

Step 2: based on the current status, the DA^{A_h} sends the INFORM messages to the applicable adjacent DAs. If its status is SL, each message is sent to a DA at level $n+1$ with the content of the corresponding CBB voltage. If the status is LS, the message is sent to the only DA at level $n-1$ along with the content of S_s. Each INFORM message is accompanied by a REQUEST message asking for performing the local voltage control.

Step 3: The adjacent DA which receives the REQUEST message changes its status based on the received information. If it receives an update on the slack node voltage, the status become *SL*; while, if it receives the update on CBBs powers, the status become LS. Furthermore, it updates its neighboring agent set N considering the information provided by the DAs that send the REQUEST messages.

Step 4: if the DA that receives the REQUEST message is A_1, the algorithm convergence criterion is checked. The convergence criterion is based on the active/reactive powers injected from the main primary substation. DA^{A_1} checks the powers variations of the main slack node with respect to the former values from the previous iteration. If this variation is lower than a specific threshold, the distributed control at the current time t converges and the active/reactive power setups of all the DESSs are updated. If this is not the case, the algorithm goes to step 1.

In order to demonstrate the message exchanges between DAs for the sweep Top-down control method, an example is presented using the same IEEE 13 nodes distribution test feeder of Fig. 4. As before, three DAs are assigned to each DESSs. Bus 2 and 7 are CBBs between. These buses are the slack nodes for area A_2 and A_3, respectively. A_1 is located at level 1 since it includes the main slack node of the system. A_2 and A_3 are located at the same level 2.

For a generic time t, DA^{A_1} performs the ALC task and it updates its own three-tuple (19) as: $DA^{A_1} : \left\{ 1, SL, \Gamma(t)^{A_1} \right\}$. Since DA^{A_1} has the SL status mode, it sends the INFORM message along with the obtained values for $V_2(t)^{A_1}$, $V_7(t)^{A_1}$ to A_2 and A_3 at level 2. Afterward, DA^{A_1} sends the REQUEST message to A_2 and A_3 and asks them to perform the ALC task. DA^{A_2} and DA^{A_3} receive the REQUEST message from A_1 with the updated values for their slack nodes voltages. Normally, the A_2 and A_3 status (γ^{A_2} and γ^{A_3}) should be changed to become similar to γ^{A_1}. However, since DA^{A_2} and DA^{A_3} have the highest level numbers, they are not able to change their status from LS to SL. The sets N^{A_2} and N^{A_3} are updated considering the received information from A_1: $N^{A_2} : \left\{ [1, V_2(t)^{A_1}, S_s(t)^{A_1}] \right\}$, $N^{A_3} : \left\{ [1, V_7(t)^{A_1}, S_s(t)^{A_1}] \right\}$. Then, DA^{A_2} and DA^{A_3} perform the ALC task locally. They update their own three-tuples (19) as $DA^{A_2} : \left\{ 1, LS, S_s(t)^{A_2}, \Gamma(t)^{A_2} \right\}$, $DA^{A_3} : \left\{ 1, LS, S_s(t)^{A_3}, \Gamma(t)^{A_3} \right\}$. Subsequently, DA^{A_2} and DA^{A_3} send the INFORM message along with the computed values for $S_s(t)^{A_2}, S_s(t)^{A_3}$ to DA^{A_1} which is located at the lower level. The INFORM messages are sent. Once DA^{A_1} receives the INFORM message from all the adjacent DAs at higher levels, it updates its neighboring agent set: $N^{A1} : \left\{ [2, V_2(t)^{A_2}, S_s(t)^{A_2}], [2, V_7(t)^{A_3}, S_s(t)^{A_3}] \right\}$. DA^{A_2} and DA^{A_3} also send the REQUEST message to DA^{A_1} asking for the ALC task. The computed losses $S_s(t)^{A_2}$ are added to the load of bus 2 and $S_s(t)^{A_3}$ is added to bus 7 before performing the ALC task. Since the ALC is to be performed by DA^{A_1} located at level 1, the convergence condition must be checked. In this respect, the DA^{A_1} verifies the main slack node injected power variations with reference to its previous value. If the variation is less than an acceptable threshold, the distributed Top-down sweep control is converged. Otherwise, the process continues until the convergence condition is met.

4. Performance evaluation

The performance evaluation of the two control methods is carried out by using a case study. For the sake of benchmarking the 123 IEEE test grids [29] is used. However, the network loads and PV injections are inferred from experimental data observed on a real ADN located in the southeast region of Switzerland. Non-dispatchable DG units (PVs) are connected to the system. Their power injections are represented by voltage-independent active

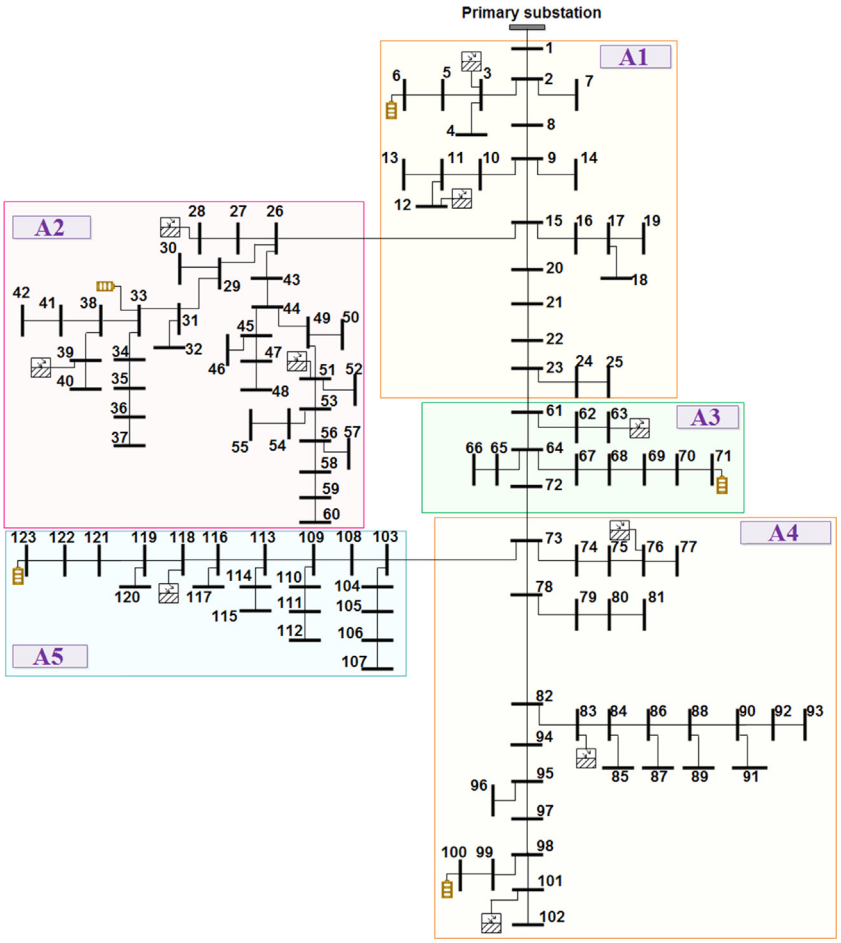

Fig. 9. Clustered IEEE 123 nodes test system.

power injections with the null reactive component[2]. The network loads are considered as voltage independent PQ absorptions. The schematic of the system, as well as the zone decomposition obtained using the method presented in Section 2, is shown in Fig. 9. The two proposed control methods are applied in the system considering five DESSs.

4.1. Network equivalent computation in Thévenin-based method

As a consequence of the network partitioning, buses 23, 26, 72, 73, are considered as CBBs. In order to validate the computation of the network equivalents, Fig. 10 shows the CBB voltage profiles in a given day with no DESS control. In particular, Fig. 10 compares the CBBs voltage magnitudes computed by a fully centralized vs. a decentralized load flow accounting for the network equivalents. Fig. 11 indicates the largest error of voltage amplitude of each CBB at each iteration of Thévenin model update for a specific time. It reflects the convergence of the process during the iterations. In this respect, Fig. 11 also shows the number of times a given load-flow needs to be computed for a given control action. It can be seen that the method converges in few iterations.

4.2. Distributed load flow solution in Top-down sweep method

Fig. 12 shows the largest error of the transferred losses among areas in each iteration for a given step time (i.e., for a given

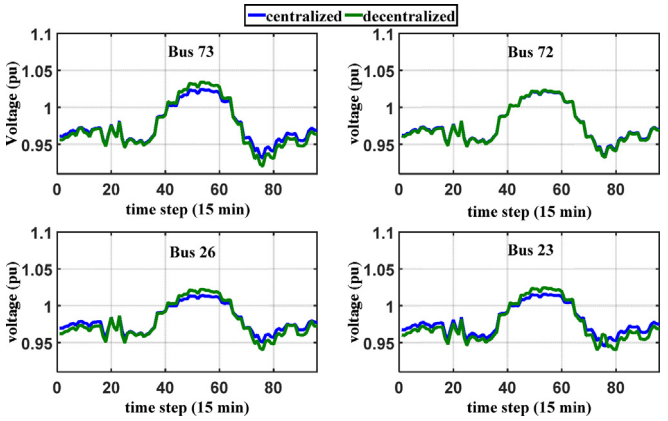

Fig. 10. *CBB voltage profiles with no DESS control actions:* comparison between a fully-centralized load flow and a local load flow with Thévenin equivalents computed using the process of Section 3.2.

[2] It should be noted that reactive power compensation from only PV inverters could be sufficient to keep the acceptable voltage profiles only in network with low R/X ratios of longitudinal line impedance parameters, whereas in ADNs normally the feeder R/X ratio might be high (see the analysis reported in [9]). Moreover, the operation of PV inverters with non-unity power factor will result in lower active power production [32]. As a result, in this paper it is considered that the control of the grid is obtained only using DESSs.

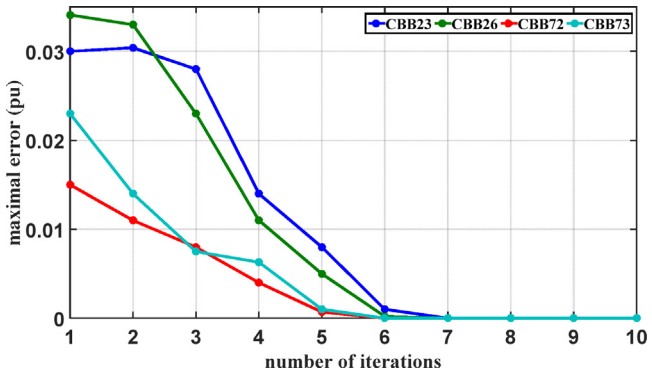

Fig. 11. The maximal error of voltage amplitude of each CBB for each iteration of Thévenin model update.

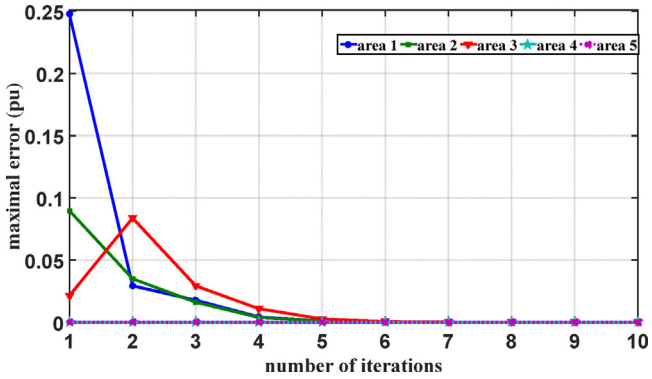

Fig. 12. Maximum errors of transferred losses among areas for each iteration of the Top-down sweep control method.

control action). The subsequent downtrend of all curves shows the convergence of the proposed method, properly. As for Fig. 11, at the same time Fig. 12 also shows the number of times a given load-flow needs to be computed for a given control action. Also in this case it can be seen that the method converges in few iterations.

It is worth mentioning that the computation time required per control action (without considering the network delays) is in the order of 0.102 s which is compatible also with quasi real-time applications (this computation time has been achieved on a workstation equipped with a 2.7 GHz quad core INTEL i7 processor, 8 GB of RAM running the Matlab® computation environment).

4.3. Performances assessment

In order to show the performances of the two control methods concerning the improvements in the voltage profiles, they are compared with the equivalent centralized control. In all the simulations, the optimization problem is solved using the YALMIP optimizer [30]. Fig. 13 shows the maximum, minimum and mean values of all the network node voltages for each 15-min period of the day, for the following cases: (i) no control on DESSs, (ii) centralized control, (iii) Thévenin-based decentralized and (iv) Top-down sweep decentralized control. As it can be seen, both decentralized control methods provide almost the same voltage improvements compared to the centralized control. As expected, the proposed decentralized methods lead to slightly worst voltage profiles in comparison with the centralized one since they do not account for VSC associated to DESSs located in areas other than the targeted one. However, they always allow limiting the voltage deviations within the range and avoiding the need of sharing all the network data. The root-mean-square error (RMSE) between centralized and decentralized control approaches is calculated using (21), for one-year voltage profile for all buses of the system. The results are shown in Fig. 14.

$$\mathrm{RMSE} = \sqrt{\frac{\sum_{t}^{T_{\max}} \sum_{i=1}^{N} \left(V_{\mathrm{centralized}}(i,t) - V_{\mathrm{decentralized}}(i,t)\right)^2}{N}} \quad (21)$$

It can be seen that the RMSE differences for the centralized vs. decentralized controls are in the order of 0.2%.

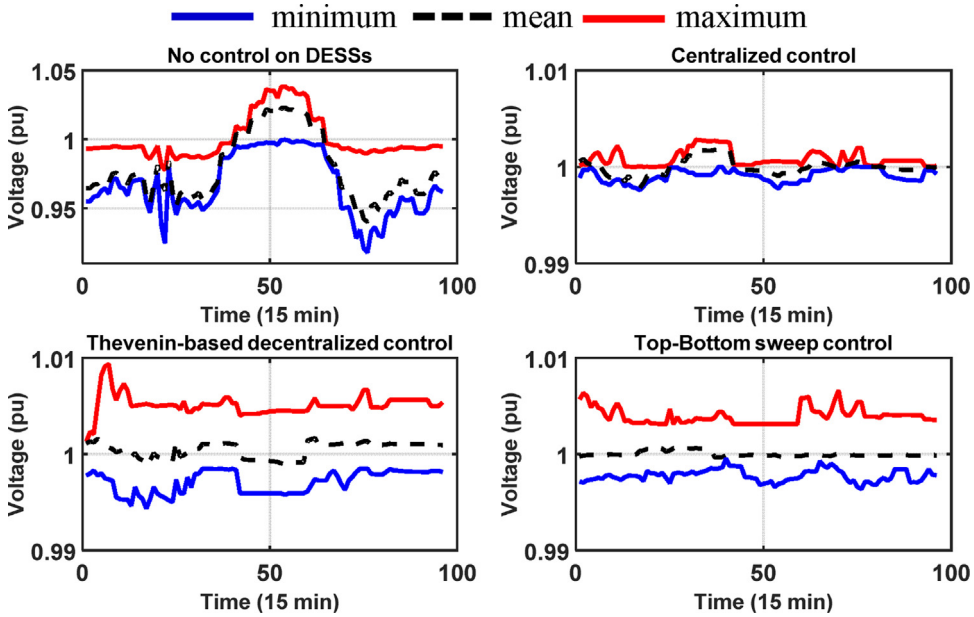

Fig. 13. Distribution of all node voltages for (i) no control, (ii) centralized control, (iii) Thévenin-based decentralized control and (iv) Top-down sweep decentralized control (the time is discretized with a 15 min interval).

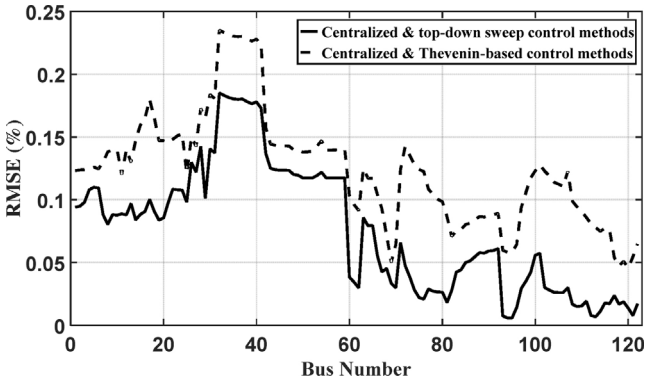

Fig. 14. RMSE between centralized and decentralized control approaches.

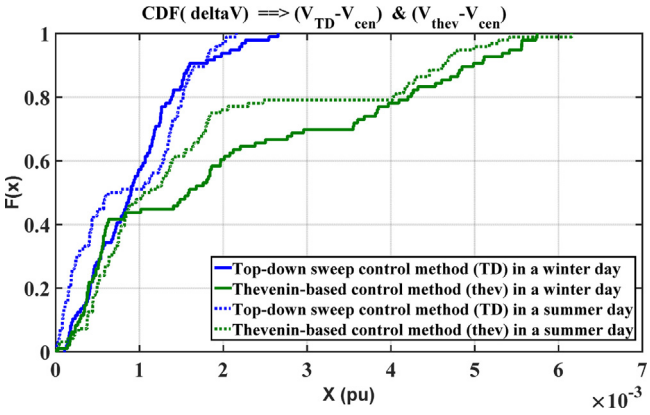

Fig. 15. CDF of the difference of the bus voltages obtained by the centralized and the two proposed decentralized control for two days in summer and winter.

By comparing the results shown in Figs. 13 and 14 associated to the two decentralized control method, it can be seen that the Top-down sweep control method performs slightly better than the Thévenin-based one. As a matter of fact, the use of the network equivalents involves the approximated representation of the external areas using, indeed, a linearized model represented by the network equivalent itself.

In order to have a more comprehensive comparison of the proposed control methods, the scenarios referring to two different days in summer and winter are considered. Fig. 15 shows the empirical cumulative distribution functions (CDFs) of the difference of the bus voltages obtained by the centralized control and the two proposed decentralized ones. Also in this case, it is observed that the behavior of the Top-down sweep control is closer to the centralized one rather than the Thévenin-based control.

Figs. 16 and 17 show the CDFs of the differences between the active and reactive power set-points of DESSs obtained by centralized control and the two proposed ones for both scenarios. It is seen that the active/reactive power set-points of DESSs in Top-down sweep control are also closer to those in the centralized one than those in the Thévenin-based control.

4.4. Optimality

It should be pointed out that the centralized control problem in our case is a convex optimization problem which always leads to a global optimal solution. Linear programming technique using voltage sensitivity coefficients are used for this purpose. Although the two proposed decentralized control algorithms are of heuristic nature providing sub-optimal solutions, they are very close to those of the equivalent centralized control problem (see Fig. 14). In addition, the convergence of the two proposed algorithms are shown in Figs. 11 and 12 for a grid with 123 nodes that exceed the size of typical distribution networks.

4.5. Agent exchanged messages

The number of exchanged messages for both proposed decentralized algorithm are shown in Fig. 18 for an entire year. It can be seen that the number of messages exchanged among the DAs in the Top-down sweep control method is much lower than the ones in the Thévenin-based control method.

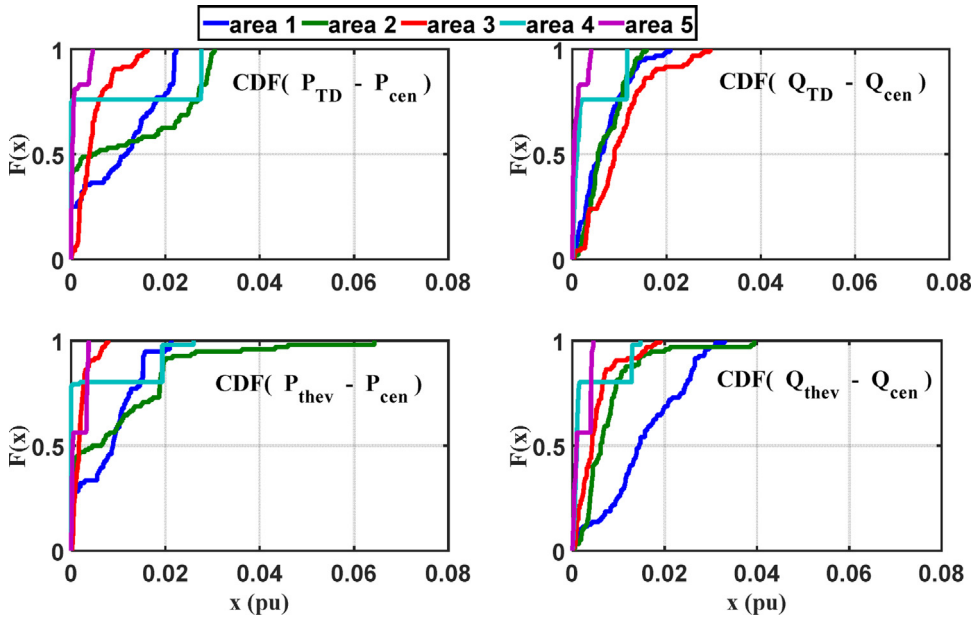

Fig. 16. CDFs of the difference between the active/reactive power set-points of DESSs obtained by Centralized (cen) and Thévenin-based (thev)/Top-down sweep (TD) control methods for a day in winter.

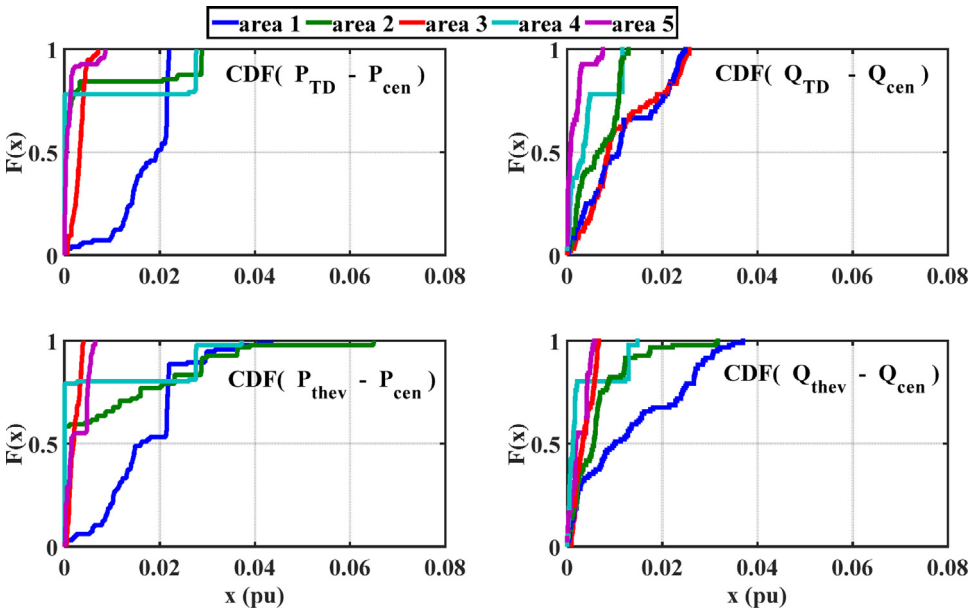

Fig. 17. CDF of the difference between the active/reactive power set-points of DESSs obtained by Centralized (cen) and Thévenin-based (thev)/Top-down sweep (TD) control methods for a day in summer.

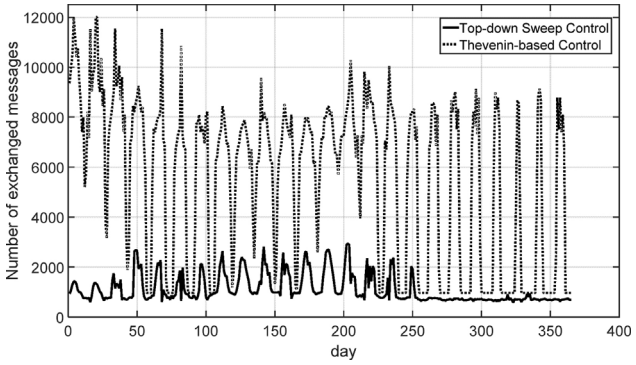

Fig. 18. Number of exchanged messaged per time interval (i.e., 15 min) for both proposed decentralized control method along an entire year.

5. Conclusions

The paper has discussed the partitioning of active distribution network (ADN) in order to define distributed voltage control processes actuated by means of a limited number of distributed energy storage systems (DESSs). In this respect, the paper has first illustrated the process to define the areas for which each DESS maximizes its influence. This clustering relies on the use of linear programming enabled by the known concept of voltage sensitivities combined with the knowledge of the statistical distributions of nodal powers that, by performing a probabilistic load flow, allows to infer the voltage influence factor (VIF) of DESS injected/absorbed powers on the grid nodal voltages.

Based on this clustering, two decentralized control strategies have been illustrated: the first one relies on the concept of Thévenin equivalents of adjacent areas whilst the second on the iterative adjustment of the power equilibrium of the areas. In both proposed control methods, the mutual influences between the areas are sacrificed in order to avoid sharing the area internal states with the others. The Thévenin-based control approach is an asynchronous algorithm in which each DESS can control its own area using the last information made available by the adjacent ones in order to infer the relevant network equivalents. Thus, the main feature of the proposed method is the independence of the voltage control for each area and the possibility for any area to join into or move back from the control scheme. On the contrary, in the Top-down sweep control approach the control of each area depends on its neighbors.

Both control algorithms are implemented in a multi-agent system environment (MAS) with different architectures of the message exchange. The paper has shown that both control methods provide almost the same voltage improvements compared to the equivalent centralized control problem. Due to the approximation considered for computing network equivalent model, the Thévenin-based control method results in slightly worse voltage profiles than the Top-down sweep control. In addition, the number of exchanged messages among the areas in the Top-down sweep method is less than the ones in the Thévenin-based method resulting in less computation burden.

Appendix A.

In the paper, it is claimed that VIF accounts for both active and reactive powers using (3). This can be numerically verified by using the simple 4 nodes test system shown in Fig. 19 with PV injections at node 3 and DESS placed at node 2. The line parameters and also load data for a specific time step are given in Tables 1 and 2. The SoC of the DESS is 0.5. For a specific time step, $VIF^{P}_{2\to4}$ and $VIF^{Q}_{2\to4}$ are calculated. By computing the electric line distance ($\alpha_{2\to4}$ and

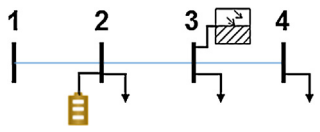

Fig. 19. Four node test system adopted to numerically verify the correctness of Eq. (3).

Table 1
4 node test load data.

Node	1	2	3	4
P (kW)	–	20	20	30
Q (kVar)	–	30	10	20

Table 2
4 node test line data.

Line	*R*	*X*	*B*
1–2	0.010014	0.023594	0.0000014
2–3	0.018183	0.018434	0.00000074
3–4	0.018546	0.014747	0.00000059

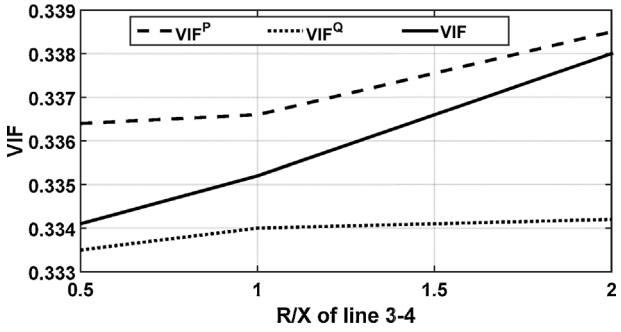

Fig. 20. Numerical verification of the VIF computation with respect to the four node test system shown in Fig. 19.

$\beta_{2\to4}$), $\mathrm{VIF}_{2\to4}$ is obtained. The $\mathrm{VIF}_{2\to4}$ as a function of R/X ratio of line 2–4 is shown in Fig. 20. It is seen that the when the R/X ratio increases (decreases), the $\mathrm{VIF}_{2\to4}$ tends to $\mathrm{VIF}^{P}_{2\to4}$ $\left(\mathrm{VIF}^{Q}_{2\to4}\right)$. From the figure, it is obvious that the $\mathrm{VIF}_{2\to4}$ accounts for both $\mathrm{VIF}^{P}_{2\to4}$ and $\mathrm{VIF}^{Q}_{2\to4}$ considering the electric line distance using (3).

References

[1] N. Hatziargyriou, Microgrids: Architectures and Control, Wiley-IEEE Press, 2014, pp. 340.
[2] F. Ren, M. Zhang, D. Sutanto, A multi-agent approach for decentralized voltage regulation in power distribution networks with distributed generators, in: International Conference on Autonomous Agents and Multi-Agent Systems, 2013, pp. 1111–1112.
[3] Voltage characteristics of electricity supplied by public distribution systems, EN Standard 50160 Release, 2010 July.
[4] A. Rogers, S.D. Ramchurn, N.R. Jennings, Delivering the smart grid: challenges for autonomous agents and multi-agent systems research, in: 26th AAAI Conf. on Artificial Intelligence, Toronto, Ontario, Canada, 2003, pp. 2166–2172.
[5] P.N. Vovos, A.E. Kiprakis, a.R. Wallace, G.P. Harrison, Centralized and distributed voltage control: impact on distributed generation penetration, IEEE Trans. Power Syst. 22 (Feb (1)) (2007) 476–483.
[6] M. Bahramipanah, M. Nick, R. Cherkaoui, M. Paolone, Network clustering for voltage control in active distribution network including energy storage systems, in: Innovative Smart Grid Technology IEEE PES Conference ISGT, Washington DC, 2015.
[7] K. Christakou, J.-Y. Le Boudec, M. Paolone, D.-C. Tomozei, Efficient computation of sensitivity coefficients of node voltages and line currents in unbalanced radial electrical distribution networks, IEEE Trans. Smart Grid 4 (2) (2012) 741–750.
[8] M.M. Begovic, A.G. Phadke, Voltage stability using sensitivity analysis, IEEE Trans. Power Syst. 7 (1) (1992) 114–123.
[9] Q. Zhou, J.W. Bialek, Simplified calculation of voltage and loss sensitivity factors in distribution networks, in: 16th Power System Computation Conference (PSCC2008), Glasgow, Scotland, 2008, pp. 14–19 (1).
[10] J. Bandler, M. El-Kady, A unified approach to power system sensitivity analysis and planning, Part I: Family of adjoint systems, in: IEEE Int. Symp. Circuits Syst., 1980, pp. 681–687.
[11] M. Nick, R. Cherkaoui, M. Paolone, Optimal allocation of dispersed energy storage systems in active distribution networks for energy balance and grid support, IEEE Trans. Power Syst. 29 (5) (2014) 2300–2310.
[12] P.F. Lyons, P. Taylor, L. Cipcigan, P. Trichakis, A. Wilson, Small scale energy zones and the impacts of high concentrations of small scale embedded generators, in: 41st International Universities Power Engineering Conference,UPEC'06, Northumbria University, UK, 2006, pp. 128–132 (2).
[13] S. Mei, X. Zhang, M. Cao, Power Grid Complexity, Springer, Tsinghua University Press, 2011.
[14] K. Christakou, D. Tomozei, M. Bahramipanah, J.-Y. Le Boudec, M. Paolone, Primary voltage control in active distribution networks via broadcast signals: the case of distributed storage, IEEE Trans. Smart Grid 5 (5) (2014) 2314–2325.
[15] A. Borghetti, M. Bosetti, S. Grillo, S. Massucco, C.A. Nucci, M. Paolone, F. Silvestro, Short-term scheduling and control of active distribution systems with high penetration of renewable resources, IEEE Syst. J. 4 (3) (2010) 313–322.
[16] J. Tang, F. Ni, F. Ponci, A. Monti, Dimension-adaptive sparse grid interpolation for uncertainty quantification in modern power systems: probabilistic power flow, IEEE Trans. Power Syst. 31 (2) (2015) 1–13.
[17] G. Carpinelli, P. Caramia, P. Varilone, Multi-linear Monte Carlo simulation method for probabilistic load flow of distribution systems with wind and photovoltaic generation systems, Renewable Energy 76 (Apr) (2015) 283–295.
[18] J. Zhao, C. Wang, B. Zhao, F. Lin, Q. Zhou, Y. Wang, A review of active management for distribution networks: current status and future development trends, Electr. Power Compon. Syst. 42 (3–4) (2014) 280–293.
[19] T. Sansawatt, L.F. Ochoa, G.P. Harrison, Smart decentralized control of DG for voltage and thermal constraint management, IEEE Trans. Power Syst. 27 (3) (2012) 1637–1645.
[20] A.E. Kiprakis, A.R. Wallace, Maximising energy capture from distributed generators in weak networks, IEE Proc. Gener. Transm. Distrib. 151 (5) (2004) 611–618.
[21] Q. Fu, L.F. Montoya, A. Solanki, A. Nasiri, V. Bhavaraju, T. Abdallah, D.C. Yu, Microgrid generation capacity design with renewables and energy storage addressing power quality and surety, IEEE Trans. Smart Grid 3 (4) (2012) 2019–2027.
[22] F.a. Viawan, A. Sannino, J. Daalder, Voltage control with on-load tap changers in medium voltage feeders in presence of distributed generation, Electr. Power Syst. Res. 77 (Aug (10)) (2007) 1314–1322.
[23] A. Vaccaro, V. Loia, G. Formato, P. Wall, V. Terzija, A self-organizing architecture for decentralized and monitoring, IEEE Trans. Ind. Inf. 11 (1) (2015) 289–298.
[24] G. Dorini, P. Pinson, H. Madsen, Chance-constrained optimization of demand response to price signals, IEEE Trans. Smart Grid 4 (4) (2013) 2072–2080.
[25] H. Sun, M. Benosman, D. Nikovski, J. Zhang, T. Takano, Y. Kojima, T. Ohno, Distributed three-phase reactive power control of distributed energy resources in distribution systems, in: International Conference on Power System Technology (POWERCON 2014), Powercon, 2014, pp. 20–22.
[26] F. Perkonigg, D. Brujic, M. Ristic, Platform for multiagent application development incorporating accurate communications modeling, IEEE Trans. Ind. Inf. 11 (3) (2015) 728–736.
[27] D. Niyato, Q. Dong, P. Wang, E. Hossain, Optimizations of power consumption and supply in the smart grid: analysis of the impact of data communication reliability, IEEE Trans. Smart Grid 4 (Mar (1)) (2013) 21–35.
[28] A. Rabiee, A. Soroudi, A. Keane, Information gap decision theory based OPF with HVDC connected wind farms, IEEE Trans. Power Syst. 30 (6) (2014) 1–11.
[29] IEEE PES Distribution System Analysis Subcommittee's Distribution Test Feeder Working Group.
[30] J. Efberg, YALMIP: A toolbox for modeling and optimization in MATLAB, in: IEEE International Symposium on Computer Aided Control Systems Design, 2004, pp. 284–289.
[31] A. Abur, A.G. Expósito, Power System State Estimation: Theory and Implementation, Power Engineering (Willis), 2004.
[32] M.N. Kabir, Y. Mishra, G. Ledwich, Z.Y. Dong, K.P. Wong, Coordinated control of grid-connected photovoltaic reactive power and battery energy storage systems to improve the voltage pro fi le of a residential distribution reeder, IEEE Trans. Ind. Inf. 10 (2) (2014) 967–977.